

Teen TITANS simulations - I. Inefficient intermediate-mass black hole seeding via stellar collisions in young massive clusters

Benedetta Mestichelli^{1,2,3}  *, Sara Rastello^{4,5}  **, Michela Mapelli^{3,6,7,8}  ***, Manuel Arca Sedda^{1,2,9} , and Marica Branchesi^{1,9}

¹ Gran Sasso Science Institute (GSSI), Viale Francesco Crispi 7, 67100, L'Aquila, Italy

² INFN, Laboratori Nazionali del Gran Sasso, I-67100 Assergi, Italy

³ Institut für Theoretische Astrophysik, Zentrum für Astronomie, Universität Heidelberg, Albert Ueberle Str. 2, D-69120 Heidelberg, Germany

⁴ Departament de Física Quàntica i Astrofísica (FQA), Universitat de Barcelona (UB), c. Martí i Franquès 1, 08028 Barcelona, Spain

⁵ Institut de Ciències del Cosmos (ICCUB), Universitat de Barcelona (UB), c. Martí i Franquès 1, 08028 Barcelona, Spain

⁶ Universität Heidelberg, Interdisziplinäres Zentrum für Wissenschaftliches Rechnen, Heidelberg, Germany

⁷ Dipartimento di Fisica e Astronomia Galileo Galilei, Università di Padova, Vicolo dell'Osservatorio 3, I-35122 Padova, Italy

⁸ INFN-Padova, Via Marzolo 8, I-35131 Padova, Italy

⁹ INAF Osservatorio Astronomico d'Abruzzo, Via Maggini, 64100 Teramo, Italy

ABSTRACT

Young massive clusters (YMCs) are dense stellar systems that provide favorable environments for frequent stellar collisions, potentially leading to the formation of very massive stars (VMSs) and seeds of intermediate-mass black holes (IMBHs). In this work, we investigate the role of repeated stellar collisions in YMCs using TITANS, a new suite of 18 N -body simulations. Our models span cluster masses of $10^5 - 10^6 M_{\odot}$, half-mass densities $\rho_h = 100 - 10^5 M_{\odot} \text{pc}^{-3}$, and include high primordial binary fractions, consistent with observations of massive stars in young clusters. Overall, our simulations assume cluster properties that are typical of YMCs in the low-redshift Universe. We find that repeated stellar collisions are efficient only in the densest clusters with short relaxation times and do not occur in systems with $\rho_h \lesssim 500 M_{\odot} \text{pc}^{-3}$ and half-mass relaxation times $t_{\text{th}} \gtrsim 1.3$ Gyr. Rapid mass segregation allows the most massive stars to sink toward the cluster center, merge, and undergo subsequent collisions, even in clusters with long core-collapse times. Nevertheless, stellar collision chains are typically triggered by the merger of a primordial binary and most often involve only two collisions. In our simulations, only three VMSs form via repeated stellar collisions and reach masses $m_* > 330 M_{\odot}$, while the majority has $m_* < 300 M_{\odot}$ and forms via primordial binary mergers. None of these objects represent viable IMBH seeds, as most of them develop helium cores in the (pulsational) pair-instability regime. We form five IMBHs from single or repeated stellar collisions involving stars at different evolutionary stages, while the dominant IMBH formation channel remains the merger of stellar-mass black holes, which produces twelve IMBHs. For densities and half-mass radii typical of local YMCs, our models show that stellar collision chains are inefficient in producing IMBHs more massive than $140 M_{\odot}$, as most collisionally formed VMSs attain masses that fall in the pair-instability regime.

1. Introduction

Young massive clusters (YMCs) are dense stellar systems with typical masses $M_{\text{cl}} \gtrsim 10^4 M_{\odot}$, half-mass radii of a few parsecs, and ages $\lesssim 100$ Myr (Portegies Zwart et al. 2010; Bastian et al. 2013). They are observed in a wide range of environments, from nearby star-forming galaxies to extreme starbursts, and are thought to represent the progenitors of globular clusters (Krumholz et al. 2019). Owing to their high stellar densities and large populations of massive stars, YMCs provide key laboratories for studying stellar dynamics, binary evolution, and the formation of compact objects, including stellar-mass black holes (BHs), gravitational-wave (GW) sources, and possible seeds of intermediate-mass black holes (IMBHs) with $m_{\text{BH}} \sim 10^2 - 10^5 M_{\odot}$ (Portegies Zwart & McMillan 2002; Portegies Zwart et al. 2004; Mapelli 2016; Di Carlo et al. 2019, 2020; Kremer et al. 2020a; Di Carlo et al. 2021; Rastello et al. 2020, 2021; Arca-Sedda et al. 2021; Rantala et al. 2024, 2025; Vergara et al. 2025).

In sufficiently dense clusters, stellar collisions are expected to occur frequently, particularly among massive stars that rapidly segregate toward the cluster center. Early studies showed that such collisions may trigger runaway growth, leading to the formation of very massive stars (VMSs) and, potentially, IMBHs. This process is especially relevant in clusters with short core-collapse times, where collisions are expected to begin before massive stars evolve into compact objects (Portegies Zwart & McMillan 2002; Portegies Zwart et al. 2004; Gaburov et al. 2008). Repeated stellar collisions have been shown to be effective in clusters with masses $> 10^5 M_{\odot}$ and central densities $> 5 \times 10^6 M_{\odot} \text{pc}^{-3}$ (Rizzuto et al. 2021; González et al. 2021; Arca Sedda et al. 2023; Rantala et al. 2024, 2025, 2026), corresponding to structural parameters that are rarely observed in local YMCs. Whether stellar collisions can efficiently promote the growth of VMSs in YMCs more commonly found in the local Universe therefore remains uncertain, partly because of the computational challenge of simulating massive clusters with high primordial binary fractions (i.e., the fraction of binaries born with the cluster).

The dynamical evolution of YMCs has been investigated using a variety of numerical techniques, including Monte Carlo

* benedetta.mestichelli@gssi.it

** sara.rastello@fqa.ub.edu

*** mapelli@uni-heidelberg.de

methods (e.g., Giersz et al. 2015; Rodriguez et al. 2022), direct N -body simulations (e.g., Wang et al. 2016; Di Carlo et al. 2020; Rastello et al. 2021; Arca Sedda et al. 2024), and hybrid N -body approaches (e.g., Wang et al. 2020a; Barber & Antonini 2025). However, most N -body studies have focused either on extremely dense clusters with relatively low total masses, adopted low primordial binary fractions, or relied on simplified prescriptions for stellar evolution. As a consequence, the combined impact of the high primordial binary fractions inferred for massive stars in local associations (Sana et al. 2012; Moe & Di Stefano 2017) and repeated stellar collisions has not yet been systematically explored in YMC models employing up-to-date single and binary stellar evolution.

In this work, we present the TITANS simulation set, a new suite of N -body simulations performed with the state-of-the-art N -body code PETAR¹. Our models span wide ranges of cluster masses ($8 \times 10^4 - 9 \times 10^5 M_\odot$) and half-mass densities ($100 - 10^5 M_\odot \text{pc}^{-3}$) adopting observation-based primordial binary fractions (Moe & Di Stefano 2017). While the ultimate goal is to compare the properties of these clusters to those of local globular clusters, we focus here on the first 20 Myr of cluster evolution (Teen TITANS), corresponding to the phase in which massive stars are still evolving into compact objects or pair-instability supernovae (PISNe). Using realistic initial conditions for YMCs (Portegies Zwart et al. 2010; Bastian et al. 2013; Krumholz et al. 2019) and stellar-evolution prescriptions that include pair-instability processes, we self-consistently study the efficiency of repeated stellar collisions, the formation and evolution of VMSs, and their impact on the BH mass spectrum in YMCs.

The paper is structured as follows. Section 2 presents the code used and the chosen initial conditions. Section 3 reports the main results on repeated stellar collisions and their final stellar products. Section 4 discusses the impact of our results on the formation of PISNe and on the BH mass distributions in our clusters. Finally, Section 5 summarizes our findings.

2. Methods

The TITANS set comprises 18 N -body simulations of star clusters in a Milky Way-like galaxy, taking into account single and binary stellar evolution, and considering a set of structural parameters compatible with observational limits in local YMCs. We perform this set of simulations with the hybrid N -body code PETAR (Wang et al. 2020a). Hybrid N -body codes are based on Hamiltonian splitting. In particular, PETAR employs the particle-tree particle-particle algorithm (P³T; Oshino et al. 2011), and the slow-down algorithmic regularization method (SDAR; Wang et al. 2020b) for an accurate and efficient treatment of binary systems and close encounters. The use of OpenMP for an efficient workload distribution across central processing units (CPUs), combined with the graphic processing unit (GPU) acceleration, contributes significantly to the strong parallel performance and scalability of PETAR. This code can include single and binary star evolution through population-synthesis algorithms. Here, we use the MOBSE population-synthesis code (Mapelli et al. 2017; Giacobbo & Mapelli 2018). PETAR can also model the effect of an external potential with GALPY (Bovy 2015).

We have performed our simulations on two servers: demoblack, hosted by the University of Padova, with 8 Nvidia Tesla V100 GPUs and 8 INTEL Xeon Platinum CPUs with 24

cores each; and bwForCluster Helix on a partition hosting 4-8 Nvidia A100 GPUs and 2 AMD EPYC CPUs with 64 cores each.

2.1. Stellar and binary evolution

In our set of simulations, we have modeled single and binary stellar evolution using the population synthesis code MOBSE (Giacobbo & Mapelli 2018, 2020). All clusters have metallicity $Z = 0.0002$, a value typical of metal-poor globular clusters (VandenBerg et al. 2013), and favoring the formation of massive compact remnants (Askar et al. 2017; Rantala et al. 2024; Arca Sedda et al. 2024; Barber & Antonini 2025).

Binary evolution processes, such as tides, mass transfer, common-envelope evolution, and GW-driven orbital decay, are implemented following the prescriptions of Hurley et al. (2002). In this work, we model the common-envelope phase using the standard $\alpha_{\text{CE}} - \lambda_{\text{CE}}$ formalism, with α_{CE} the fraction of orbital energy used to unbind the envelope, and λ_{CE} a parameter characterizing the envelope's binding energy and structure. In particular, we adopt $\alpha_{\text{CE}} = 1$, while λ_{CE} is calculated according to Claeys et al. (2014).

For core-collapse supernovae (SNe), we rely on the delayed formalism by Fryer et al. (2012). This model adopts a convection-enhanced neutrino-driven mechanism for the SN explosion, and the revival of the shock wave happens ~ 250 ms after the collapse. With this prescription the minimum BH mass is $3 M_\odot$.

After the SN explosion, compact remnants receive a natal kick modeled following Giacobbo & Mapelli (2020):

$$v_{\text{kick}} = f_{\text{H05}} \frac{\langle m_{\text{NS}} \rangle}{m_{\text{rem}}} \frac{m_{\text{ej}}}{\langle m_{\text{ej}} \rangle}, \quad (1)$$

where $\langle m_{\text{NS}} \rangle$ and $\langle m_{\text{ej}} \rangle$ are the average neutron-star mass and ejecta mass, computed from a population of isolated neutron stars with metallicities representative of the Milky Way, m_{rem} is the mass of the compact object, and m_{ej} is the ejected mass. f_{H05} is a number randomly drawn from a Maxwellian distribution with one-dimensional root mean square $\sigma_{\text{kick}} = 265 \text{ km s}^{-1}$, derived from the proper motions of young Galactic pulsars (Hobbs et al. 2005). This formalism implies that BHs forming through direct collapse receive a null natal kick. In this study we do not include a formalism for the natal spin of BHs.

For PISNe and pulsational PISNe we have used the fitting formulas reported in the appendix of Mapelli et al. (2020), based on Woosley (2017). When the helium core mass of a star, $m_{\text{He,f}}$, is between 32 and $64 M_\odot$, it undergoes a pulsational PISN. A PISN is triggered instead when $64 \leq m_{\text{He,f}} \leq 135 M_\odot$. For isolated single stellar evolution at the metallicity adopted in our simulations, this corresponds to a range in the zero-age main-sequence mass $140 \lesssim m_{\text{ZAMS}} \lesssim 260 M_\odot$. When $m_{\text{He,f}} > 135 M_\odot$, the star directly collapses into a BH.

2.2. Compact object mergers in PETAR

In dense star clusters with a high fraction of primordial binaries, collisions and mergers between stars and BHs can happen frequently (see e.g. Rastello et al. 2025). The outcome of such interactions is still unclear. On the one hand, we expect that stars with $m_* < 10 M_\odot$ would accrete little or no mass on the BH (Kremer et al. 2020b). On the other, simulations from Schröder et al. (2020) show that common envelope events between a star and a BH can lead to the accretion of the stellar core on the BH

¹ <https://github.com/lwang-astro/PeTar>

and to the ejection of the envelope. Moreover, various dynamical studies (Kiroğlu et al. 2025a,b) have found that BHs can accrete mass from repeated collisions with stars in a dense cluster. As a consequence, previous works (Banerjee 2021; Rizzuto et al. 2021; Arca Sedda et al. 2024) have assumed a fraction of stellar accreted mass on the BH $f_c > 0$. In this work, we have adopted a more conservative approach, assuming $f_c = 0$.

In PETAR, GW-driven mergers are modeled by evolving the semi-major axis and eccentricity of the binary according to the formalism of Peters (1964). A binary is considered to merge when its GW timescale becomes shorter than its integration timestep, which depends on the strength of nearby perturbations and the binary’s slowdown factor. Once this condition is met, PETAR evolves the binary’s position to the merger time, allowing us to locate binary BH (BBH) mergers within the cluster.

2.3. External potential

We model the influence of an external galactic potential using the GALPY package (Bovy 2015). Specifically, we assume that the star clusters reside in a Milky Way-like galaxy and follow a circular orbit around the Galactic center at a radius of 8 kpc with a velocity of 220 km s⁻¹, corresponding to the Solar neighborhood. For the galactic potential, we adopt the MWPotential2014 model, which includes a Miyamoto-Nagai potential for the disk (Miyamoto & Nagai 1975), a spherical bulge component based on a truncated power-law density profile (Hernquist 1990), and a Navarro-Frenk-White potential for the dark matter halo (Navarro et al. 1996).

2.4. Initial conditions

The initial conditions of our simulations are generated using MCLUSTER (Küpper et al. 2011). We adopt initial cluster masses in the range $M_{cl} \in [8 \times 10^4, 9 \times 10^5] M_\odot$, with positions and velocities sampled from a King density profile (King 1966) characterized by a central potential parameter $W_0 = 6$ and half-mass radii $r_h \in [1, 5]$ pc. These values are consistent with those measured for YMCs in the local Universe (Portegies Zwart et al. 2010; Bastian et al. 2013; Krumholz et al. 2019). The initial density at half-mass radius ρ_h of our clusters is between 100 and $10^5 M_\odot \text{pc}^{-3}$ and the half-mass relaxation time t_{th} (Spitzer 1988) is between 100 Myr and 3 Gyr. A summary of the initial conditions for our suite of simulations is provided in Table 1.

Stellar masses are sampled from a Kroupa initial mass function (Kroupa 2001) between 0.08 and 150 M_\odot . We assume that the primordial binary fraction depends on the primary mass of the star, according to the prescriptions in Moe & Di Stefano (2017). The global binary fraction f_b is defined as $f_b = N_b / (N_s + N_b)$ and its value is ~ 0.23 across all the models, corresponding to $\sim 38\%$ of stars in a primordial binary. Binaries are initialized with distributions of mass ratio, semi-major axis, and eccentricity motivated by the intrinsic properties of massive binaries inferred by Sana et al. (2012). We extend the orbital period range up to 10^5 days to include wide, non-interacting binaries. In addition, the mass-ratio distribution is extrapolated to $q < 0.1$ to allow for extreme mass-ratio systems.

Figure 1 shows the location of our simulations in the $N - \rho_h$ and $N - f_b$ planes, where N is the number of particles. We compare our models with state-of-the-art studies performed using Monte Carlo methods (e.g., Askar et al. 2017; Rodriguez et al. 2019; Maliszewski et al. 2022), direct N -body simulations (e.g., Mapelli et al. 2013; Mapelli 2016; Wang et al. 2016; Arca Sedda

et al. 2024; Rantala et al. 2024), and hybrid N body approaches (e.g., Wang et al. 2021; Rastello et al. 2025). The main novelty of the TITANS simulation set lies in the fact that, although it explores a region of the $N - \rho_h$ parameter space already covered by previous studies, it does so adopting a global primordial binary fraction f_b that has so far been investigated almost exclusively using Monte Carlo techniques (Askar et al. 2017; Maliszewski et al. 2022). Importantly, our simulations sample a region of parameter space that is representative of YMCs and globular clusters in the local Universe, whose typical densities are $\lesssim 10^6 M_\odot \text{pc}^{-3}$.

The total simulated time for each cluster, t_{sim} , exceeds 20 Myr in all cases. For the first 20 Myr, the evolution of each star cluster is tracked in greater detail, with output snapshots recorded every 0.125 Myr. In this work, we focus on the first 20 Myr of cluster evolution, corresponding to the lifetime of a $\sim 12 M_\odot$ star; hence, we expect that all BHs have formed by this time and most SNe have already taken place. Moreover, within 20 Myr, the densest clusters contract and undergo core collapse (Spitzer 1988). After $t_{sim} > 20$ Myr, output snapshots are recorded every 1 Myr.

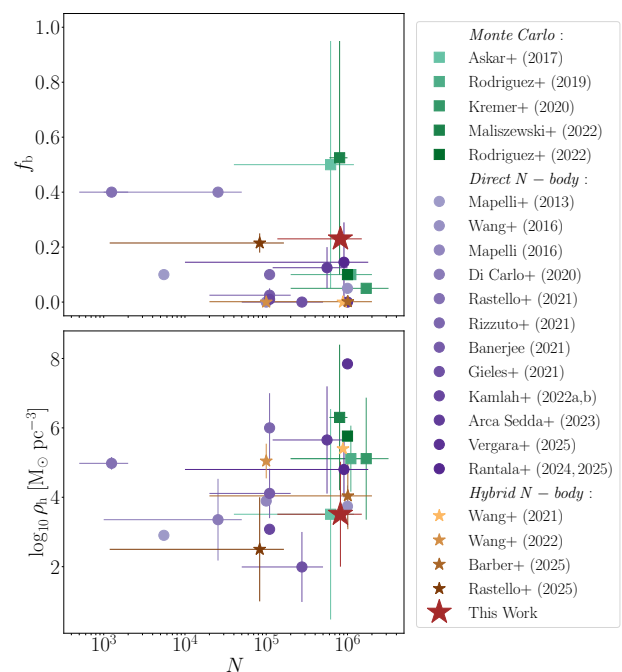


Fig. 1: Initial binary fraction (top row) and density at half-mass radius (bottom row) as a function of the initial number of stars, for Monte Carlo (green squares), direct N -body (violet circles) and hybrid N -body simulations (brown stars). The TITANS simulations are represented by a red star.

2.5. Properties of stellar collisions

Stellar collisions and repeated stellar collisions have been extensively investigated as formation channels of IMBH progenitors (Portegies Zwart & McMillan 2002; Portegies Zwart et al. 2004; Giersz et al. 2015; Mapelli 2016; Di Carlo et al. 2021; González et al. 2021; Rizzuto et al. 2021; Kritos et al. 2023; Reinoso et al. 2023; Arca sedda et al. 2024; Rantala et al. 2024, 2025; Vergara et al. 2025; Paiella et al. 2025). In this work, we explore the properties of repeated stellar collisions in YMCs with a high f_b , and features typical of local star clusters.

Table 1: Initial conditions of the TITANS set

Model	N 10^3	M_{cl} $10^5 M_{\odot}$	N_{b} 10^3	r_{h} pc	ρ_{h} $10^3 M_{\odot} \text{pc}^{-3}$	t_{rh} Gyr	$t_{\text{sim}}/t_{\text{rh}}$	$t_{\text{sim}}/t_{\text{cc}}$
T1	136.9	0.8	25.8	1	9.7	0.1	51	255
T2	195.4	1.2	36.7	5	0.1	1.3	4.3	21
T3	372.9	2.2	70.3	2	3.3	0.4	4.7	23.7
T4	407	2.4	76.7	2	3.7	0.4	0.05	0.3
T5	411.1	2.5	77.5	2	3.7	0.4	0.7	3.3
T6	528.4	3.2	99.7	5	0.3	1.9	0.3	1.3
T7	600.8	3.6	113.3	5	0.4	2	1	5.3
T8	825.7	4.9	155.6	5	0.5	2.3	0.1	0.5
T9	823.2	5	155.3	1	59.1	0.2	0.1	0.5
T10	850.7	5.1	160.4	5	0.5	2.3	0.3	2
T11	1000	6.1	190.3	1	9.1	0.6	0.4	2
T12	1230.6	7.4	232	2	11.1	0.7	0.1	0.5
T13	1262.1	7.6	237.8	5	0.7	2.7	0.02	0.1
T14	1314.2	8	247.9	2	11.9	0.7	0.03	0.1
T15	1343.2	8.1	253.1	2	12	0.7	0.03	0.1
T16	1430.8	8.6	270	1	102.7	0.3	0.07	0.3
T17	1461.4	8.8	275.3	5	0.8	2.9	0.1	0.6
T18	1508.7	9.1	284.5	5	0.9	2.9	0.02	0.1

Notes. Column 1: name of the model. Column 2: number of stars $N = N_{\text{s}} + 2 N_{\text{b}}$. Column 3: cluster mass. Column 4: number of binary systems. Column 5: half-mass radius of the cluster. Column 6: density at half-mass radius of the cluster. Column 7: half-mass relaxation time (Spitzer 1988). Column 8 and 9: fraction of simulated time with respect to the relaxation time t_{rh} and the core-collapse time $t_{\text{cc}} \sim 0.2 t_{\text{rh}}$.

Here, we define a stellar collision chain as a sequence containing at least two stellar collisions or mergers. Throughout the paper, we use the term “stellar collision” in a broad sense, referring both to mergers of binary components and to direct collisions between unbound stars. We quantify the efficiency of repeated stellar collisions as $\eta_{\text{rep}} = N_{\text{ch,rep}}/M_{\text{cl}}$, where $N_{\text{ch,rep}}$ is the number of stellar collision chains identified in each cluster. Figure 2 represents schematically a stellar collision chain, initiated either by the merger of a primordial or dynamical binary, or by a stellar collision (i.e. a binary that is not born with the cluster), or by a stellar collision. The resulting star will itself either form a dynamical binary that will later merge, or collide with another star. We expect this process to re-iterate itself for several times, especially in dense clusters with small relaxation times. When the remnants from two or more chains merge, we compute $N_{\text{ch,rep}}$ as the sum of the length of the chains.

We also examine how repeated stellar collisions affect the mass spectrum of VMSs and IMBHs. All through this study, we define VMSs as stars whose mass exceeds the upper limit of the adopted initial mass function ($m_{*} > 150 M_{\odot}$), and IMBHs as BHs with $m_{\text{BH}} > 100 M_{\odot}$.

3. Results

In the following Sections, we discuss the properties of repeated stellar collisions (Sec. 3.1), and their impact on the formation of VMSs (Sec. 3.2). We will show our results considering only the first 20 Myr of evolution of each cluster.

3.1. Repeated stellar collisions

3.1.1. Impact of the host environment

Figure 3 shows the efficiency of repeated stellar collisions as a function of $\rho_{\text{h}}/(\rho_{\text{h},3} M_{\text{cl},5})$, with $\rho_{\text{h},3} = 10^3 M_{\odot} \text{pc}^{-3}$ and $M_{\text{cl},5} = 10^5 M_{\odot}$. As defined in Sec. 2.5, the efficiency of repeated collisions

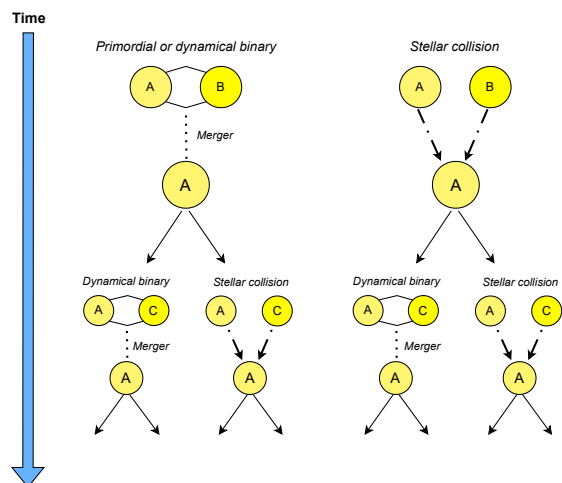


Fig. 2: Schematic representation of a stellar collision chain. We show on the left a chain initiated by the merger of the components of a binary (either primordial or dynamically formed). On the right we show instead a chain initiated by an hyperbolic stellar collision.

sions is $\eta_{\text{rep}} = N_{\text{ch,rep}}/M_{\text{cl}}$, where $N_{\text{ch,rep}}$ is the number of stellar collision chains identified in each cluster. As cluster density increases, so does the efficiency of repeated collisions. We fit the data with a linear relation in logarithmic space, obtaining

$$\log_{10}(\eta_{\text{rep}}) \approx 0.8 \log_{10}\left(\frac{\rho_{\text{h}}}{\rho_{\text{h},3} M_{\text{cl},5}}\right) - 1.4 \quad \text{with } \rho_{\text{h}} \gtrsim 500 M_{\odot} \text{pc}^{-3}. \quad (2)$$

The intrinsic scatter around the best-fit relation is $\sigma_{\text{int}} \sim 0.3$ dex. This trend indicates that a high cluster density is a key requirement for the onset of multiple stellar collisions. Moreover, we find that repeated collisions occur only for $\rho_h \gtrsim 500 M_\odot \text{pc}^{-3}$.

An opposite trend is observed with respect to the relaxation time t_{rh} . At fixed density, clusters with shorter relaxation times exhibit a higher efficiency of repeated collisions. In fact, an efficient formation of merger chains requires a mass-segregation time $t_{\text{DF}} \sim \langle m \rangle t_{\text{rh}} / m_{\text{bin}}$ shorter than the lifetime of the stars involved, $t_{\text{DF}} < t_{\text{end}}$, where the average stellar mass is $\langle m \rangle \sim 0.6 M_\odot$ and the binary mass satisfies $m_{\text{bin}} \leq 300 M_\odot$. For the most massive binaries in our clusters ($m_{\text{bin}} = 300 M_\odot$, $m_1 = m_2 = 150 M_\odot$), the stellar lifetime is $t_{\text{end}} \sim 3$ Myr, corresponding to a maximum relaxation time $t_{\text{rh}} \sim 1.5$ Gyr. Less massive binaries will require longer times to segregate to the cluster center.

As shown in Table 1, more than half of the TITANS models have $t_{\text{rh}} \lesssim 1.5$ Gyr. As a consequence, despite their relatively long core-collapse times ($t_{\text{cc}} > 20$ Myr), these clusters can form stellar collision chains because the most massive primordial binaries segregate rapidly to the center. Once in the core, these binaries merge, and the increasing central density of massive stars favors the formation of new dynamical binaries or direct stellar collisions. This result is consistent with the findings of Rantala et al. (2025) on the key role of primordial binaries in clusters with long core-collapse times. In contrast, clusters with $t_{\text{rh}} \gtrsim 1.5$ Gyr require more time for binaries to segregate and interact; by the time they reach the core, the most massive stars are often already evolved or have died as compact objects, reducing the efficiency of chain formation.

Figure 4 shows the number of stellar collision chains $N_{\text{ch,rep}}$ as a function of the normalized half-mass density $\rho_h / \rho_{h,3}$ and of the length of the chains themselves. The minimum density required for a chain to form increases with the number of collisions it contains: chains with two collisions appear at $\rho_h \sim 500 M_\odot \text{pc}^{-3}$, chains with three collisions require densities of $\sim 4000 M_\odot \text{pc}^{-3}$ and chains with four or more collisions form only at densities above $\sim 10^4 M_\odot \text{pc}^{-3}$. In all cases, $N_{\text{ch,rep}}$ increases approximately linearly with density. However, the slope decreases for longer chains, indicating that extended collision sequences are rare even in clusters with high densities and low relaxation times. As a result, the contribution of long collision chains to $N_{\text{ch,rep}}$ and η_{rep} remains limited. In the densest model of our suite (T16, $\rho_h \sim 10^5 M_\odot \text{pc}^{-3}$), 70% of the chains contain two collisions, 20% contain three collisions, and only 10% involve more than four collisions. We point out that models T2, T6, and T7, do not produce any stellar collision chains. Models T3, T10, T13, and T18 instead produce a single chain each ($N_{\text{ch,rep}} = 1$), always containing two collisions.

Finally, we compute the fraction of stellar collision chains whose first merger involves the components of a primordial binary. This fraction is 100% up to $\rho_h \sim 10^4 M_\odot \text{pc}^{-3}$ and remains above $\sim 72\%$ at higher densities. When the first collision does not involve a primordial binary merger, it results either from a hyperbolic encounter or from a highly eccentric collision between a low-mass main-sequence (MS) star and one component of a primordial binary. In the latter case, the perturber can be either a single star or a component of a low-mass primordial binary, which is disrupted during the interaction. Owing to the small mass ratio between the perturber and the massive primordial binary component, this first merger does not significantly alter the orbit of the primordial binary, whose components subsequently merge.

Overall, these results highlight that stellar collision chains are efficient only in clusters with $\rho_h \gtrsim 10^4 M_\odot \text{pc}^{-3}$ and with $t_{\text{rh}} \lesssim 300$ Myr and that, even then, they mostly contain two collisions and are triggered by a primordial binary merger. In Secs. 3.2 and 4.3 we will explore the effect of these findings on VMSs and IMBHs.

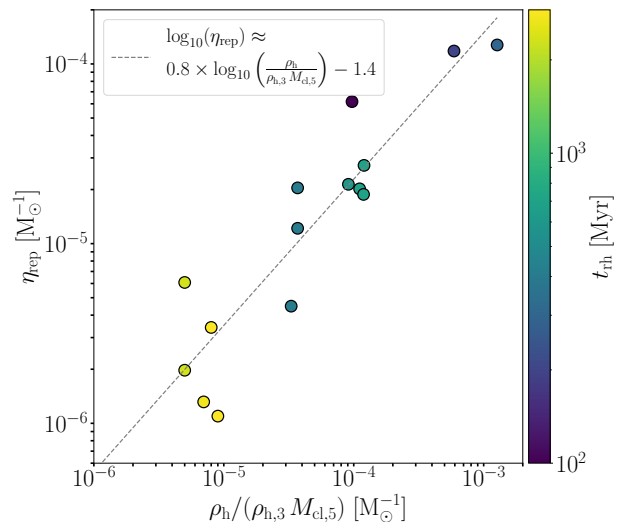


Fig. 3: Efficiency of repeated stellar collisions η_{rep} as a function of the half-mass density ρ_h , normalized by $\rho_{h,3}$ and $M_{\text{cl},5}$. The points are colored as a function of the cluster initial relaxation time t_{rh} .

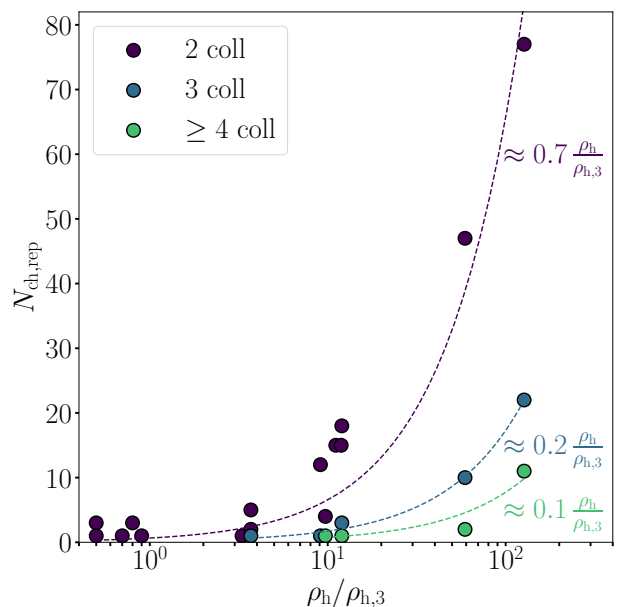


Fig. 4: Number of stellar collision chains $N_{\text{ch,rep}}$ as a function of the normalized density at half-mass radius $\rho_h / \rho_{h,3}$. In violet we represent the number of chains containing two collisions, in blue the number of chains containing three collisions and in green the number of chains containing four or more collisions. The dashed lines and annotations represent the linear fits of the points.

3.1.2. Stellar properties

Figure 5 shows the stellar types of primary stars involved in repeated collisions in the simulated models, colored by the relaxation time of their host cluster. We do not show the stellar types of secondaries because in all models $\geq 93\%$ stars are in their MS. Moreover, we do not show models T2, T6 and T7 since they do not produce stellar collision chains. In about half of the simulated models, the primary stars involved in repeated stellar collisions are preferentially in their MS. With increasing t_{th} the fraction of evolved stars involved in repeated stellar collisions grows. In fact, longer relaxation times correspond to longer mass segregation timescales and, as a consequence, stars are more evolved by the time they reach the dense cluster center and take part in the collisions. Moreover, low densities lead to bigger intervals of time between consecutive collisions, allowing the stars to evolve. We move from model T1 ($t_{\text{th}} \sim 100$ Myr) with $\sim 77\%$ primaries in the MS, to model T17 ($t_{\text{th}} \sim 3$ Gyr) with only $\sim 17\%$ primaries in their MS. Models T3, T10 and T18, appearing as outliers, produce only one chain of stellar collisions.

Figure 6 shows the primary masses of all the stars involved in repeated stellar collisions. The bars contain all the mass values, while the rectangles contain 50% of the data. We see that the bulk values of primary masses do not strongly depend on the properties of the host clusters. Dense clusters with $t_{\text{th}} \leq 700$ Myr (e.g. T1, T9, T14, T16) have larger bulk values ($50 \lesssim m_1 \lesssim 130 M_{\odot}$) and they cover broader mass intervals. In fact, repeated stellar collisions are more frequent in dense clusters with low relaxation times (Fig. 3), and they mainly involve stars in their MS (Fig. 5). Model T9 spans a primary mass interval extending up to $350 M_{\odot}$, due to the long chains of repeated stellar collisions forming in this cluster. Models T13 and T18, appearing as outliers, have $N_{\text{ch,rep}} = 1$. We also represent here the maximum mass reached in our clusters through stellar collision chains; we see that the highest values are reached in models T1, T9 and T16, which have the lowest relaxation times. For secondary masses, we find that the bulk values are usually below $m_2 \lesssim 25 M_{\odot}$ if $t_{\text{th}} \gtrsim 500$ Myr.

3.2. Very massive stars

We summarize here the properties of the VMSs ($m_* > 150 M_{\odot}$) forming in our simulated clusters. Table 2 lists, for each model, the number of VMSs, their maximum mass, and their formation channels.

The number of VMSs generally increases with cluster mass, consistently with the fact that their dominant formation pathway is the merger of primordial binaries, whose abundance scales with M_{cl} . In the densest clusters with short relaxation times, stellar collision chains play a non-negligible role in VMS formation. This is especially evident in models T1, T9, and T16, where more than 25% of VMSs originate from repeated collisions. Models T9 and T16 form a larger number of VMSs than clusters of comparable mass because repeated stellar collisions are more efficient in these systems. In all the other models, the VMSs counted in $N_{\text{VMS, coll}}$ form predominantly ($> 82\%$) via primordial binary mergers. This result highlights again the key role of primordial binaries in driving the early dynamical and stellar evolution of YMCs with properties in line with low-redshift observations (Portegies Zwart et al. 2010; Rantala et al. 2025). We find that binary evolution also contributes to VMS formation: in particular, stable mass transfer can produce stars with masses up to $\sim 200 M_{\odot}$. Across all clusters, the median VMS mass shows only a weak dependence on cluster properties and remains in the

range $160 - 200 M_{\odot}$. All VMSs identified in our simulations are still on the MS, as their formation typically occurs through stellar collisions involving young stars.

Table 2 also reports the maximum stellar mass attained in each simulation. Figure 7 shows it as a function of the initial half-mass density of the clusters. Since VMSs form early during cluster evolution ($t < 5$ Myr), this trend remains unchanged when considering the density at the time of their formation. For clusters with $\rho_{\text{h}} \lesssim 10^4 M_{\odot} \text{pc}^{-3}$ and $t_{\text{th}} > 300$ Myr, the maximum stellar mass is nearly independent of density and relaxation time, lying between 215 and $300 M_{\odot}$, with stochastic variations reflecting the collisional nature of VMS formation. In all these cases, VMSs originate from primordial binary mergers. In models with $\rho_{\text{h}} \gtrsim 10^4 M_{\odot} \text{pc}^{-3}$ and $t_{\text{th}} \lesssim 300$ Myr, the maximum stellar mass exceeds $330 M_{\odot}$. The three stars in this regime form in models T1, T9, and T16 through stellar collision chains.

Finally, the last column of Table 2 reports the number of VMSs that merge with a stellar-mass BH. Appendix A discusses the final fate of these stars and the impact of our initial prescriptions. The subsequent evolution of VMSs is instead addressed in Sec. 4.

4. Discussion

In the following, we discuss the impact of stellar collisions and repeated stellar collisions on PISNe (Sec. 4.1), and the mass distribution of BHs (Sec. 4.2). We focus particularly on the formation and properties of IMBHs in Sec. 4.3. Also here, we consider only the first 20 Myr of evolution of each cluster, unless otherwise specified. In Sec. 4.4 we report the caveats and limitations of our models.

4.1. Pair-instability supernovae

We expect that stellar collisions increase the number of stars entering the PISN mass range relative to predictions from the initial mass function, potentially enhancing the rates of PISNe and pulsational PISNe in metal-poor star clusters compared to the field.

In our simulations, most PISNe originate either from stars that are born directly within the PISN mass range or from stars that enter it following a primordial binary merger. Since none of the PISN progenitors escape from the clusters, both formation channels scale with the cluster mass M_{cl} . This behavior is confirmed in Fig. 8, which shows that both the total number of PISNe and the fraction produced through stellar collisions correlate strongly with M_{cl} . The contribution of stellar collisions to the total PISN population is above $\sim 70\%$, with large scatter among clusters with similar properties, reflecting the stochastic nature of stellar collisions and massive binary evolution. Only four PISNe (3 in model T9, 1 in model T16) form via repeated stellar collisions. We find that $\geq 90\%$ of our PISNe explode as single stars, while the remaining part is found in a binary system. The only exception is model T1, where 50% of the PISNe explode in a binary. This difference is driven by small-number statistics, as T1 is the least massive cluster in our sample and forms only two PISNe.

Figure 8 also shows the expected number of PISNe from an isolated population of single stars, assuming that the PISN mass gap starts at $\sim 140 M_{\odot}$ (Spera & Mapelli 2017; Giacobbo et al. 2018). We find that the number of stars born in our clusters within the PISN mass range is consistent with the isolated case. However, stellar collisions (primarily in the form of primordial binary mergers) and, to a lesser extent, repeated stellar

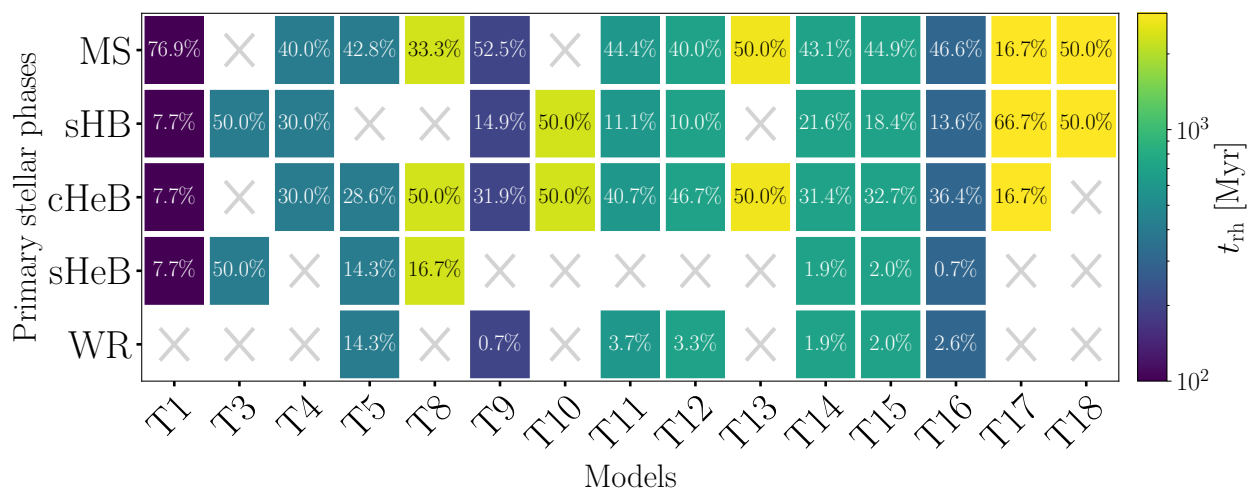


Fig. 5: Primary stellar type of stars involved in repeated collisions. The x axis shows the simulated models. The stellar phases on the y axis are: MS, shell hydrogen burning (sHB), core helium burning (cHeB), shell helium burning (sHeB) and Wolf-Rayet star (WR). The color represents the relaxation time at half-mass radius t_{th} .

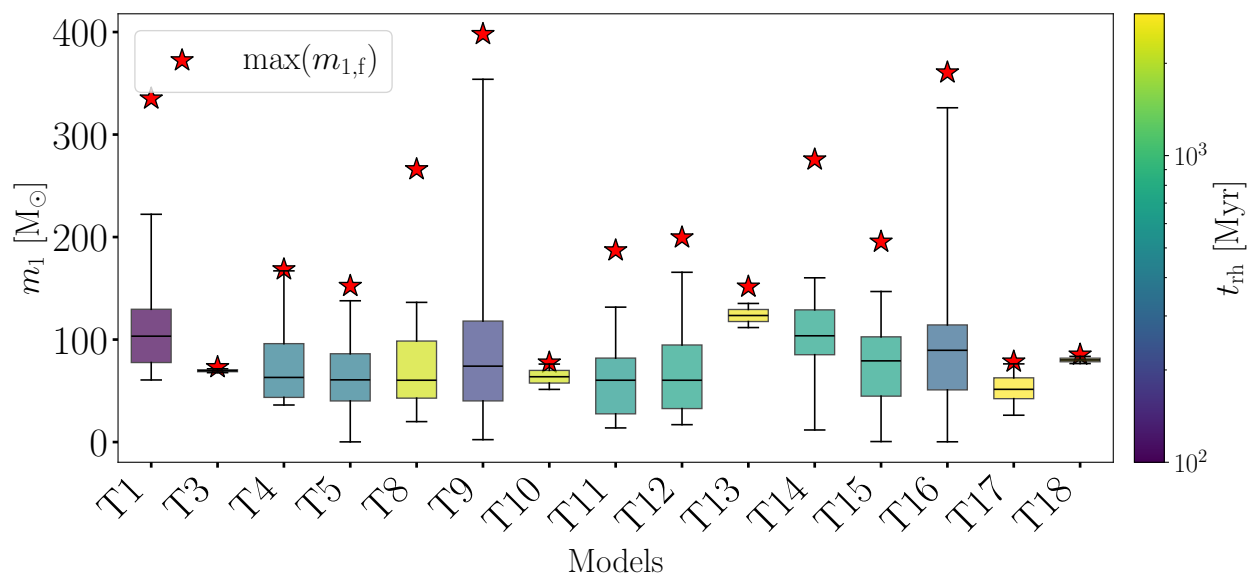


Fig. 6: Distribution of primary mass m_1 of stars involved in repeated stellar collisions for each simulated model. The color represents the relaxation time at half-mass radius t_{th} . We show with a red star the maximum mass of the product of a stellar collision chain in each model.

collisions, allow additional stars to enter the PISN regime, increasing the total number of PISNe. As a result, in most of our models the total number of PISNe forming in star clusters is up to one order of magnitude larger than expected for an isolated single stellar population.

In our simulations, the PISN mass gap corresponds to $140 \lesssim m_* \lesssim 400 M_{\odot}$ considering the final stellar mass before the explosion, with the bulk of the population $< 289 M_{\odot}$ (e.g., Arca Sedda et al. 2024). We expect these results to be robust against uncertainties in stellar-wind prescriptions owing to the low metallicity adopted in this work (Simonato et al. 2025).

Finally, we find that $\geq 70\%$ of the VMSs formed in the clusters explode as PISNe. The remaining VMSs typically lose a substantial fraction of their mass and collapse into stellar-mass black holes with $m_{\text{BH}} < 100 M_{\odot}$ as a result of pulsational PISNe (see Sec. 4.2), or are removed through collisions with stellar-

mass black holes (see Appendix A). The only exception is model T1, in which $\sim 33\%$ of the VMSs die as PISNe.

4.2. Black hole mass distribution

To assess the impact of single and repeated stellar collisions on the BH mass spectrum, we focus on three models with different values of density and relaxation time (T2, T13, T16). Figure 9 shows the corresponding BH mass distributions, highlighting the contributions from stellar collisions and stellar collision chains. As expected, the total number of BHs increases with the mass of the host cluster, ranging from 721 to 2892 BHs in the most massive model (T16). In parallel, the number of BHs originating from single stellar collisions also grows with cluster mass, accounting for $\sim 28 - 35\%$ of the total BH population (Di Carlo et al. 2019; Arca Sedda et al. 2024), reflecting the increasing

Table 2: Properties of VMSs in the simulated models

Model	N_{VMS}	$m_{\text{VMS,max}}$ M_{\odot}	$N_{\text{VMS,bin}}$	$N_{\text{VMS,coll}}$	$N_{\text{VMS,repcoll}}$	$N_{\text{BH,coll}}$
T1	6	334.9	0	3	3	1
T2	10	212.8	1	9	0	0
T3	13	213.2	1	12	0	1
T4	15	261.8	3	11	1	0
T5	22	282.8	2	20	0	0
T6	27	270.1	4	23	0	0
T7	18	276.8	3	15	0	0
T8	36	266	6	30	0	0
T9	46	397.7	3	32	11	0
T10	24	264.2	5	19	0	1
T11	28	270.2	5	22	1	1
T12	42	256.1	9	33	0	0
T13	45	266.5	7	38	0	0
T14	56	290	4	50	2	0
T15	40	268.3	4	36	0	1
T16	84	391.9	7	61	16	4
T17	58	268.5	13	45	0	0
T18	50	270.8	3	47	0	0

Notes. Column 1: name of the model. Column 2: total number of VMSs. Column 3: maximum mass of VMSs in each cluster. Column 4: number of VMSs due to binary evolution processes. Column 5: number of VMSs due to single collisions. Column 6: number of VMSs due to chains of collisions. Column 7: number of VMSs colliding with a stellar-mass BH.

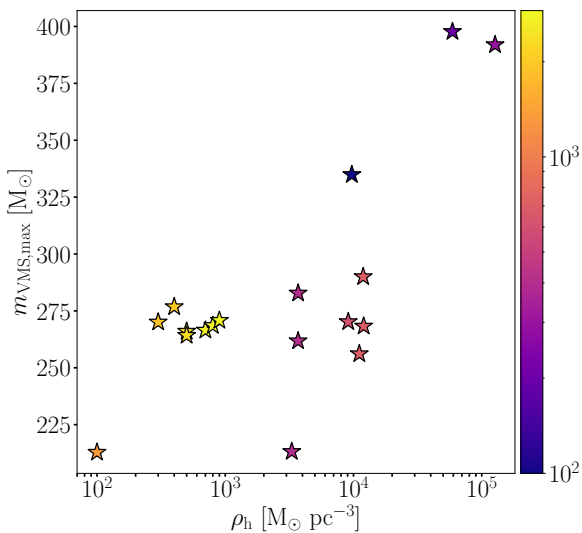


Fig. 7: Relation between the maximum VMS mass $m_{\text{VMS,max}}$ and the initial density at half-mass radius ρ_h . The colors used represent the initial relaxation time t_{th} .

number of massive stars and primordial binaries in more massive systems. A qualitatively different behavior is observed only in model T16, the densest cluster in our suite ($\rho_h \sim 10^5 M_{\odot} \text{pc}^{-3}$) with a short relaxation time ($t_{\text{th}} = 300 \text{ Myr}$). In this case, a non-negligible fraction (3%) of BHs forms from the collapse of the final products of stellar collision chains.

The BH mass distributions are characterized by a pronounced primary peak at $m_{\text{BH}} \sim 5 M_{\odot}$ and a secondary pile-up at $\sim 35 M_{\odot}$. The latter is primarily driven by the adopted prescriptions for pulsational PISNe (Woosley 2017; Spera & Mapelli 2017), which, at the low metallicity of our models, induce strong mass loss and effectively funnel BH remnants toward masses be-

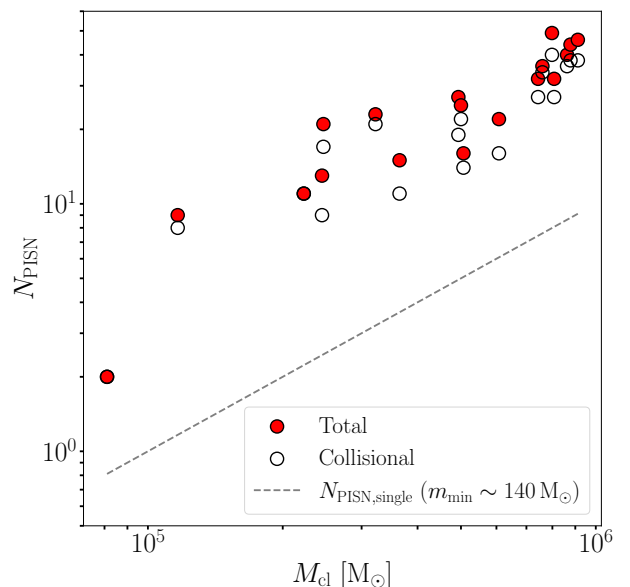


Fig. 8: Number of PISNe as a function of the cluster mass M_{cl} . The filled red points represent the total number; the empty black points represent instead the number of PISNe due to collisions. As a comparison we plot the number of PISNe expected from single stellar evolution $N_{\text{PISN,single}}$.

low $m_{\text{BH}} \lesssim 50 M_{\odot}$. In addition, the large primordial binary fractions adopted in our simulations, combined with the preference for short initial orbital separations (Sana et al. 2012), promote efficient envelope stripping and mass loss during binary evolution, further contributing to the accumulation of BHs in this mass range.

BHs formed from single stellar collisions broadly follow the overall mass distribution, with a comparatively smaller contribu-

tion to the low-mass peak. In contrast, BHs originating from stellar collision chains predominantly populate the $\sim 35 M_{\odot}$ peak. This behavior indicates that, even when stellar progenitors undergo substantial mass growth through repeated collisions, the combined effects of pulsational PISNe and binary interactions efficiently limit the final BH mass. Finally, the number of BHs with $m_{\text{BH}} \geq 60 M_{\odot}$ is small, marking the lower edge of the PISN mass gap in our models. Nevertheless, we find that the population of BHs in the upper-mass gap grows with cluster mass. In model T13 a single IMBH forms; this case is discussed in detail in Sec. 4.3. In model T16, instead, the enhanced impact of stellar collisions and collision chains leads to the formation of 85 BHs with masses $60 \leq m_{\text{BH}} \leq 90 M_{\odot}$.

4.3. Intermediate-mass black holes

In the following, we consider two families of IMBHs ($m_{\text{BH}} > 100 M_{\odot}$): those that arise from stellar collisions and those that originate from BBH mergers. These two classes are not mutually exclusive, as IMBHs formed through BBH mergers may have stellar progenitors that themselves experienced stellar collisions (Arca Sedda et al. 2023; Arca sedda et al. 2024; Rantala et al. 2025).

Among the 18 TITANS simulations that reached $t_{\text{sim}} = 20$ Myr, five produce an IMBH through a purely stellar channel. All these IMBHs have masses $\leq 107 M_{\odot}$ and share the same formation pathway: a MS star merges with a cHeb companion, resulting in a star whose helium core remains below the threshold for pulsational PISN (Di Carlo et al. 2020; Kremer et al. 2020a; Arca-Sedda et al. 2021), and that will later collapse into an IMBH. In four models (T12, T13, T14, T18), this merger happens only once and between the components of a primordial binary. Model T9, however, exhibits a more complex evolution: the initial merger product (between a MS and a cHeb star) subsequently undergoes two additional collisions with MS stars (see Fig. 10).

By contrast, none of the VMSs formed in our clusters collapses into an IMBH. Instead, most VMSs either explode as PISNe (Sec. 4.1), leave behind stellar-mass BHs (Sec. 4.2), or are stripped of mass through collisions with compact remnants (Appendix A). This means that, unless substantial material is accreted during BH-star collisions ($f_c = 0$) and within the model uncertainties, the seeding of IMBHs through the collapse of a VMS is not possible in star clusters with initial $\rho_h \lesssim 10^5 M_{\odot} \text{pc}^{-3}$ and $t_{\text{rh}} > 100$ Myr.

We also assess the impact of stellar collisions on BBH mergers that produce IMBHs. For this analysis we consider the entire simulated duration of each model, and not just the first 20 Myr. This choice introduces a bias toward simulations evolved for longer times, but it enables us to capture the full role of primordial binaries, stellar collisions and stellar collision chains across all clusters. Throughout the following discussion, we describe only IMBHs resulting from a single BBH merger, as relativistic kicks are not taken into account in PETAR (see Sec. 4.4). We identify twelve IMBHs formed through BBH mergers, including four produced outside their parent cluster, all with masses $\leq 140 M_{\odot}$. Among these, five have one progenitor produced by a primordial stellar merger, one has a progenitor that experienced repeated collisions, and one has both progenitors originating from primordial stellar mergers. As a consequence, we find that stellar mergers (T10, T12, T17) and mass transfer (T8) in primordial binaries can facilitate the formation of IMBHs through BBH mergers even before core collapse, when it is expected that high cluster densities promote the BBH coupling and eventual merger.

We note that most of the IMBHs formed in our simulations, whether originating from the stellar channel or from BBH mergers, lie within the PISN mass gap ($60 \lesssim m_{\text{BH}} \lesssim 120 M_{\odot}$). The high primordial binary fractions adopted in this study enable YMCs to produce IMBHs in, or just above, the PISN range through both stellar interactions and BBH mergers. However, the relatively low escape velocities of these clusters, combined with the absence of mechanisms to grow a seed above the PISN mass range, prevent the formation of substantially larger IMBHs. As a result, our simulations indicate that YMCs with properties consistent with those observed in the local Universe are unlikely to produce large IMBHs even in the presence of high primordial binary fractions.

4.4. Caveats

The initial conditions adopted in this work (see Table 1) are broadly consistent with observations of YMCs in the local Universe. We also assume high primordial binary fractions (Moe & Di Stefano 2017) and employ a state-of-the-art treatment of single and binary stellar evolution. Nevertheless, our results rely on a number of assumptions that are worth discussing.

First, we assume that all clusters form through the monolithic collapse of a molecular cloud. In reality, star clusters may form from clouds with significant departures from spherical symmetry or through the hierarchical assembly of smaller sub-clusters (e.g., Sánchez & Alfaro 2009; Ballone et al. 2020; Torniamenti et al. 2021). Recent studies have shown that hierarchical assembly can significantly enhance the rate of repeated stellar collisions, favoring the formation of large ($\sim 10^3 M_{\odot}$) IMBH seeds (Rantala et al. 2024, 2025, 2026). Our results should therefore be regarded as conservative with respect to scenarios in which cluster substructure persists during the early stages of evolution.

Second, the properties of YMCs may evolve with redshift. Recent observations with JWST have begun to reveal extremely compact and massive stellar systems in the early Universe (Adélaïde et al. 2026 and references therein), characterized by high stellar densities and short relaxation times. Such environments would likely experience an enhanced efficiency of stellar collisions and collision chains, potentially allowing the formation of VMSs with helium cores above the PISN regime and increasing the probability of IMBH seed formation. For example, Vergara et al. (2025) recently showed that a cluster with $\rho_h \sim 10^8 M_{\odot} \text{pc}^{-3}$ and $t_{\text{rh}} \sim 7$ Myr forming in the early Universe can produce a VMS as massive as $50,000 M_{\odot}$ collapsing in an IMBH.

Third, our conclusions depend on the adopted prescriptions for stellar and binary evolution. In particular, the stellar mass range associated with the PISN and pulsational PISN regimes is uncertain and model dependent. Alternative prescriptions based on Spera & Mapelli (2017) predict a narrower PISN mass range, which could allow IMBH seeds to form even under initial conditions similar to those explored here. Additional uncertainties arise from the treatment of stellar winds, mass transfer, and envelope stripping in massive binaries, all of which can affect the final masses of collision products and compact remnants. We also point out that in our work we have not considered collision-induced mass-loss (Gaburov et al. 2010; Ramírez-Galeano et al. 2025).

We also assume that the fraction of stellar mass accreted by a BH during a collision is zero ($f_c = 0$). Adopting a higher accretion efficiency can significantly alter the outcomes of stellar-BH collisions and would lead to the formation of up to nine additional IMBHs in our simulations (see Appendix A).

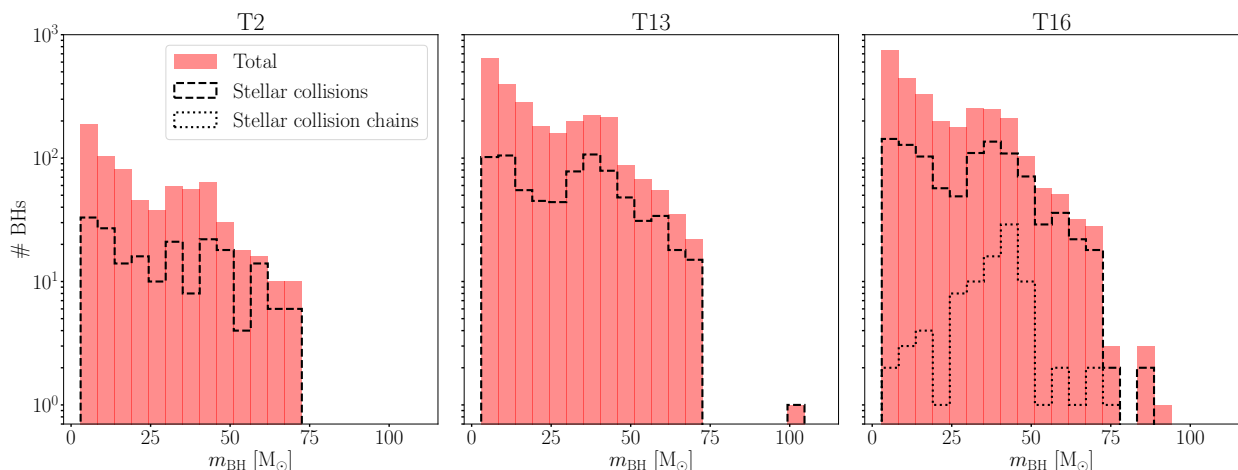


Fig. 9: BH mass distribution for models T2, T13 and T16. We show in red the mass distribution of all BHs; the black dashed line shows the BHs formed through single stellar collisions; the black dotted line shows instead the BHs formed through repeated stellar collisions.

Finally, *PETAR* does not include relativistic recoil kicks following GW mergers. As a consequence, in Sec. 4.3 we consider only first-generation BBH mergers as viable IMBH formation channels. Given the relatively low escape velocities of our clusters, we expect most successive-generation merger remnants to be ejected. A follow-up study will explore the long-term evolution of compact objects and their merger products in greater detail.

5. Summary

We have investigated the impact and properties of repeated stellar collisions in YMCs over the first 20 Myr of evolution using the new set of direct N -body simulations *TITANS*. These models span a wide range of cluster masses and densities consistent with low-redshift YMCs and include a high, observation-based fraction of primordial binaries (Fig. 1).

We find that the efficiency of repeated stellar collisions increases with increasing half-mass density ρ_h and decreasing half-mass relaxation time t_{rh} (Fig. 3). Clusters with $\rho_h \gtrsim 10^4 M_\odot \text{pc}^{-3}$ and dynamical friction times $t_{rh} \lesssim 300$ Myr efficiently form stellar collision chains, although these typically involve only two collisions and are generally triggered by primordial binary mergers. Only a minority of chains in the densest clusters undergo three or more collisions (Fig. 4).

The evolutionary stage of the primary stars involved in repeated collisions depends strongly on the cluster relaxation time (Fig. 5). In particular, the fraction of primaries on the MS decreases from $\sim 77\%$ in the model with the shortest relaxation time (T1) to $\sim 17\%$ in the model with the longest relaxation time (T17). The masses of primaries in collision chains vary accordingly, with typical values $50 \lesssim m_1 \lesssim 130 M_\odot$ in dense clusters with $t_{rh} \leq 700$ Myr (Fig. 6).

Very massive stars are predominantly formed via primordial binary mergers and typically remain below $300 M_\odot$. Only in the densest clusters with the shortest relaxation times (T1, T9, T16) do repeated stellar collisions produce VMSs with masses up to $\sim 400 M_\odot$ (Fig. 7). As a consequence, the number of VMSs generally scales with cluster mass. Most of these stars either explode as PISNe or leave behind stellar-mass BHs with $m_{BH} < 50 M_\odot$, and none represent viable IMBH seeds.

The number of PISNe in our clusters grows with cluster mass (Fig. 8), as the dominant formation channels involve massive stars and primordial binary mergers, whose frequency increases with cluster mass. Compared to an isolated population of single stars, which is expected to produce PISNe only for zero-age MS masses above $140 M_\odot$, our clusters generate up to an order of magnitude more PISNe owing to the contribution of stellar collisions.

The BH mass distribution exhibits a primary peak at $\sim 5 M_\odot$ and a secondary peak at $\sim 35 M_\odot$ (Fig. 9). Stellar collision chains contribute mainly to the secondary peak, indicating that pulsational PISNe and binary interactions effectively regulate the final BH masses, even when stellar progenitors experience substantial mass growth through repeated collisions.

Finally, we find that IMBHs form through two main channels: (i) collisions, either single or repeated, between a cHeb star and a MS star (Fig. 10), producing five IMBHs, and (ii) single BBH mergers, producing twelve IMBHs. In both cases, the resulting IMBHs remain relatively small ($m_{BH} < 140 M_\odot$). Both formation pathways are strongly enhanced by the high primordial binary fraction, which promotes stellar collisions, mass transfer episodes, and the assembly of merging BBHs.

In summary, adopting initial conditions compatible with low-redshift YMCs and state-of-the-art N -body modeling, we find that repeated stellar collisions can be efficient when mass-segregation times are sufficiently short. However, collision chains typically involve only two events and are largely driven by primordial binaries. Within our conservative modeling assumptions ($f_c = 0$), VMSs do not act as viable IMBH seeds, and only collisions between stars at different evolutionary stages can produce small IMBH progenitors. While this work focuses on the early evolution of YMCs, our simulations are ongoing and have already reached $t_{sim} > 1$ Gyr for the least dense clusters. A follow-up study will investigate the long-term evolution of compact objects and compact binary mergers in these systems.

Acknowledgements. MM acknowledges financial support from the European Research Council for the ERC Consolidator grant DEMOBLACK, under contract no. 770017. MM also acknowledges financial support from the German Excellence Strategy via the Heidelberg Cluster of Excellence (EXC 2181 - 390900948) STRUCTURES. MAS acknowledges funding from the European Union's Horizon 2020 research and innovation programme under the Marie Skłodowska-Curie grant agreement No. 101025436 (project GRACE-BH) and from the MERAC Foundation. MB and MAS acknowledge support from the

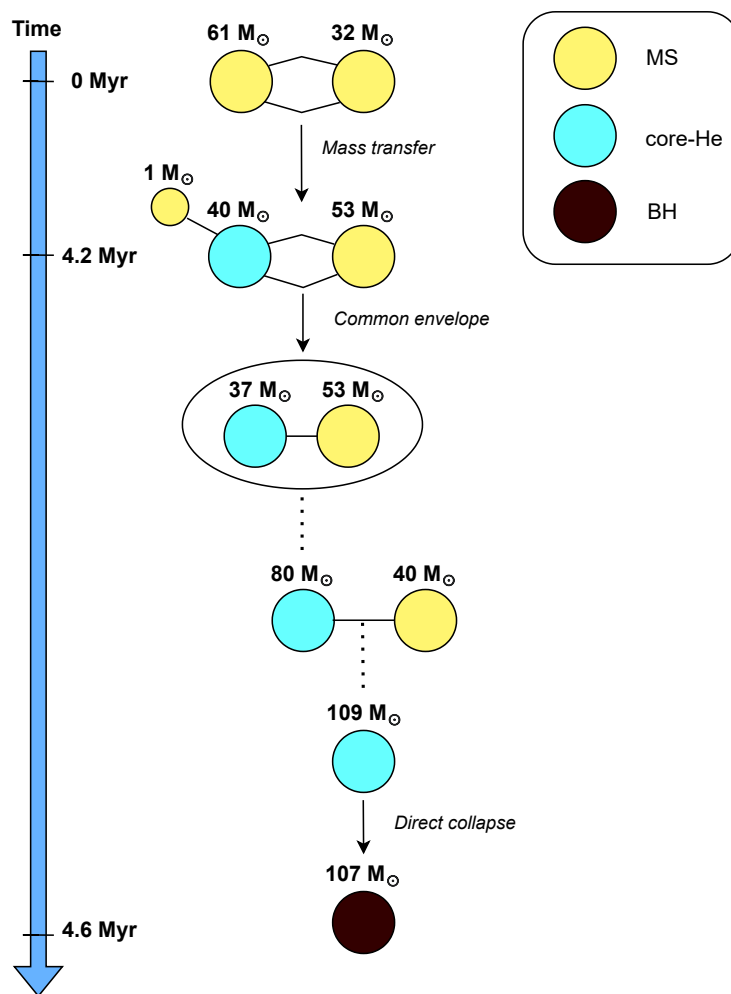


Fig. 10: Formation pathway of the IMBH in model T9.

Astrophysics Center for Multi-messenger Studies in Europe (ACME), funded under the European Union’s Horizon Europe Research and Innovation Program, Grant Agreement No. 101131928. SR acknowledges financial support from the Beatriu de Pinós postdoctoral fellowship program under the Ministry of Research and Universities of the Government of Catalonia (Grant Reference No. 2021 BP 00213). The authors acknowledge support by the state of Baden-Württemberg through bwHPC and the German Research Foundation (DFG) through grants INST 35/1597-1 FUGG and INST 35/1503-1 FUGG. This research made use of NumPy (Harris et al. 2020), SciPy (Virtanen et al. 2020), PANDAS (pandas development team 2020). For the plots we used MATPLOTLIB (Hunter 2007). Our simulations made use of the N -body code PETAR (Wang et al. 2020a and <https://github.com/lwang-astro/PeTar>) and of the population-synthesis code MOBSE (Mapelli et al. 2017; Giacobbo et al. 2018 and https://gitlab.com/micmap/mobse_open).

References

- Adélaïde, C., Angela, A., Vasily, K., et al. 2026, [arXiv e-prints](https://arxiv.org/abs/2601.16281), arXiv:2601.16281
- Arca Sedda, M., Kamlah, A. W. H., Spurzem, R., et al. 2024, *MNRAS*, 528, 5119
- Arca Sedda, M., Kamlah, A. W. H., Spurzem, R., et al. 2023, *MNRAS*, 526, 429
- Arca-Sedda, M., Rizzuto, F. P., Naab, T., et al. 2021, *ApJ*, 920, 128
- Askar, A., Szkudlarek, M., Gondek-Rosińska, D., Giersz, M., & Bulik, T. 2017, *MNRAS*, 464, L36
- Ballone, A., Mapelli, M., Di Carlo, U. N., et al. 2020, *MNRAS*, 496, 49
- Banerjee, S. 2021, *MNRAS*, 500, 3002
- Barber, J. & Antonini, F. 2025, *MNRAS*, 538, 639
- Bastian, N., Cabrera-Ziri, I., Davies, B., & Larsen, S. S. 2013, *MNRAS*, 436, 2852
- Bovy, J. 2015, *ApJS*, 216, 29
- Claeys, J. S. W., Pols, O. R., Izzard, R. G., Vink, J., & Verbunt, F. W. M. 2014, *A&A*, 563, A83
- Di Carlo, U. N., Giacobbo, N., Mapelli, M., et al. 2019, *MNRAS*, 487, 2947

- Di Carlo, U. N., Mapelli, M., Giacobbo, N., et al. 2020, *MNRAS*, 498, 495
- Di Carlo, U. N., Mapelli, M., Pasquato, M., et al. 2021, *MNRAS*, 507, 5132
- Fryer, C. L., Belczynski, K., Wiktorowicz, G., et al. 2012, *ApJ*, 749, 91
- Gaburov, E., Gualandris, A., & Portegies Zwart, S. 2008, *MNRAS*, 384, 376
- Gaburov, E., Lombardi, Jr., J. C., & Portegies Zwart, S. 2010, *MNRAS*, 402, 105
- Giacobbo, N. & Mapelli, M. 2018, *MNRAS*, 480, 2011
- Giacobbo, N. & Mapelli, M. 2020, *ApJ*, 891, 141
- Giacobbo, N., Mapelli, M., & Spera, M. 2018, *MNRAS*, 474, 2959
- Giersz, M., Leigh, N., Hypki, A., Lützgendorf, N., & Askar, A. 2015, *MNRAS*, 454, 3150
- González, E., Kremer, K., Chatterjee, S., et al. 2021, *ApJ*, 908, L29
- Harris, C. R., Millman, K. J., van der Walt, S. J., et al. 2020, *Nature*, 585, 357
- Hernquist, L. 1990, *ApJ*, 356, 359
- Hobbs, G., Lorimer, D. R., Lyne, A. G., & Kramer, M. 2005, *MNRAS*, 360, 974
- Hunter, J. D. 2007, *Computing in Science & Engineering*, 9, 90
- Hurley, J. R., Tout, C. A., & Pols, O. R. 2002, *MNRAS*, 329, 897
- King, I. R. 1966, *AJ*, 71, 64
- Kıroğlu, F., Kremer, K., Biscoveanu, S., González Prieto, E., & Rasio, F. A. 2025a, *ApJ*, 979, 237
- Kıroğlu, F., Kremer, K., & Rasio, F. A. 2025b, arXiv e-prints, arXiv:2509.05415
- Kremer, K., Spera, M., Becker, D., et al. 2020a, *ApJ*, 903, 45
- Kremer, K., Ye, C. S., Rui, N. Z., et al. 2020b, *ApJS*, 247, 48
- Kritov, K., Berti, E., & Silk, J. 2023, *Phys. Rev. D*, 108, 083012
- Kroupa, P. 2001, *MNRAS*, 322, 231
- Krumholz, M. R., McKee, C. F., & Bland-Hawthorn, J. 2019, *ARA&A*, 57, 227
- Küpper, A. H. W., Maschberger, T., Kroupa, P., & Baumgardt, H. 2011, *MNRAS*, 417, 2300
- Maliszewski, K., Giersz, M., Gondek-Rosinska, D., Askar, A., & Hypki, A. 2022, *MNRAS*, 514, 5879
- Mapelli, M. 2016, *MNRAS*, 459, 3432
- Mapelli, M., Giacobbo, N., Ripamonti, E., & Spera, M. 2017, *MNRAS*, 472, 2422
- Mapelli, M., Spera, M., Montanari, E., et al. 2020, *ApJ*, 888, 76
- Mapelli, M., Zampieri, L., Ripamonti, E., & Bressan, A. 2013, *MNRAS*, 429, 2298
- Miyamoto, M. & Nagai, R. 1975, *PASJ*, 27, 533
- Moe, M. & Di Stefano, R. 2017, *ApJS*, 230, 15
- Navarro, J. F., Frenk, C. S., & White, S. D. M. 1996, *ApJ*, 462, 563
- Oshino, S., Funato, Y., & Makino, J. 2011, *PASJ*, 63, 881
- Paiella, L., Arca Sedda, M., Mestichelli, B., & Ugolini, C. 2025, arXiv e-prints, arXiv:2511.00200
- pandas development team, T. 2020, pandas-dev/pandas: Pandas
- Peters, P. C. 1964, *Physical Review*, 136, 1224
- Portegies Zwart, S. F., Baumgardt, H., Hut, P., Makino, J., & McMillan, S. L. W. 2004, *Nature*, 428, 724
- Portegies Zwart, S. F. & McMillan, S. L. W. 2002, *ApJ*, 576, 899
- Portegies Zwart, S. F., McMillan, S. L. W., & Gieles, M. 2010, *ARA&A*, 48, 431
- Ramírez-Galeano, L., Charbonnel, C., Fragos, T., et al. 2025, *A&A*, 699, A223
- Rantala, A., Lahén, N., Naab, T., Escobar, G. J., & Iorio, G. 2025, arXiv e-prints, arXiv:2506.04330
- Rantala, A., Naab, T., & Lahén, N. 2024, *MNRAS*, 531, 3770
- Rantala, A., Naab, T., Lahén, N., et al. 2026, arXiv e-prints, arXiv:2601.07917
- Rastello, S., Iorio, G., Gieles, M., & Wang, L. 2025, arXiv e-prints, arXiv:2509.12318
- Rastello, S., Mapelli, M., Di Carlo, U. N., et al. 2020, *MNRAS*, 497, 1563
- Rastello, S., Mapelli, M., Di Carlo, U. N., et al. 2021, *MNRAS*, 507, 3612
- Reinoso, B., Klessen, R. S., Schleicher, D., Glover, S. C. O., & Solar, P. 2023, *MNRAS*, 521, 3553
- Rizzuto, F. P., Naab, T., Spurzem, R., et al. 2021, *MNRAS*, 501, 5257
- Rodriguez, C. L., Weatherford, N. C., Coughlin, S. C., et al. 2022, *ApJS*, 258, 22
- Rodriguez, C. L., Zevin, M., Amaro-Seoane, P., et al. 2019, *Phys. Rev. D*, 100, 043027
- Sana, H., de Mink, S. E., de Koter, A., et al. 2012, *Science*, 337, 444
- Sánchez, N. & Alfaro, E. J. 2009, *ApJ*, 696, 2086
- Schröder, S. L., MacLeod, M., Loeb, A., Vigna-Gómez, A., & Mandel, I. 2020, *ApJ*, 892, 13
- Simonato, F., Torniamenti, S., Mapelli, M., et al. 2025, *A&A*, 703, A215
- Spera, M. & Mapelli, M. 2017, *MNRAS*, 470, 4739
- Spitzer, L. S. 1988, *Dynamical Evolution of Globular Clusters*
- Torniamenti, S., Ballone, A., Mapelli, M., et al. 2021, *MNRAS*, 507, 2553
- VandenBerg, D. A., Brogaard, K., Leaman, R., & Casagrande, L. 2013, *ApJ*, 775, 134
- Vergara, M. C., Askar, A., Kamlah, A. W. H., et al. 2025, *A&A*, 704, A321
- Virtanen, P., Gommers, R., Burovski, E., et al. 2020, *scipy/scipy: SciPy 1.6.0*
- Wang, L., Fujii, M. S., & Tanikawa, A. 2021, *MNRAS*, 504, 5778
- Wang, L., Iwasawa, M., Nitadori, K., & Makino, J. 2020a, *MNRAS*, 497, 536
- Wang, L., Nitadori, K., & Makino, J. 2020b, *MNRAS*, 493, 3398
- Wang, L., Spurzem, R., Aarseth, S., et al. 2016, *MNRAS*, 458, 1450
- Woosley, S. E. 2017, *ApJ*, 836, 244

Appendix A: Impact of the chosen accretion fraction f_c

In the following we explore the impact of the assumed accretion fraction f_c in case of a collision or merger between a star and a BH.

Table 2 shows that nine VMSs in our set of simulations collide with a BH. Because of our assumption of $f_c = 0$, no mass is accreted by a BH in case of a collision with a star. A clear example of this scenario, where the VMS is the result of a stellar collision chain, is shown in Fig. A.1. In most cases, the VMSs form either via binary evolution, accreting mass from the companion which will later become a BH, or via a primordial binary merger. Once the companion is a BH, the star transfers its mass, which is lost, bringing away angular momentum and widening the orbit. The merger finally happens when the star expands enough.

If we assumed $f_c = 0.5$ (e.g. Arca Sedda et al. 2024), we could obtain nine more IMBHs up to $m_{\text{BH}} \sim 215 M_\odot$ in our simulations, deriving from the merger of binaries formed by a VMS and a BH. We also expect that the accretion of stellar mass from a VMS onto a stellar-mass BH might lead to a significant spin-up of the BH (Kiroğlu et al. 2025a,b).

To evaluate the impact of our prescription on the BH population in our models, we have also looked into all the collisions involving a primary star and a secondary BH. We show in Fig. A.2 the distribution of the mass ratio $q = m_{\text{BH}}/m_*$ for all the simulated models. We see that usually q is smaller than ~ 0.4 and that it shows a peak at $q \lesssim 0.2$. Even though the amount of spin-up via stellar collisions is still largely unknown, we can expect that, in case of small mass ratios such as these, both the mass and spin of the BH would increase. Consequently, our adopted choice of $f_c = 0$ effectively represents a conservative scenario, as it minimizes the mass growth of BHs via stellar collisions in our models. Figure A.2 also shows the distribution of BH masses after collisions assuming $f_c = 0.5$. Most BHs in this case have final masses $\lesssim 50 M_\odot$, with a peak around $m_{\text{BH,f}} \sim 20 M_\odot$. The only BHs reaching the IMBH regime originate from collisions in which the primary was a VMS; these cases are listed in Table 2.

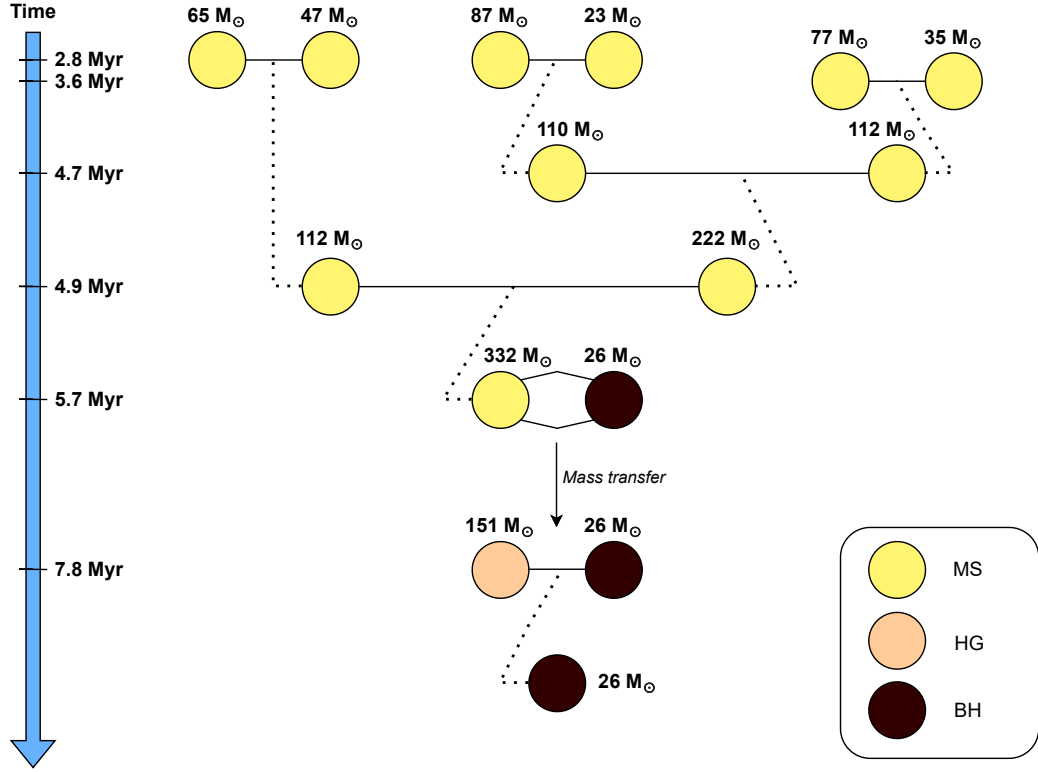


Fig. A.1: Stellar collision chain leading to a VMS-BH merger in model T1. In this case $f_c = 0$ and the final BH does not accrete mass from the VMS.

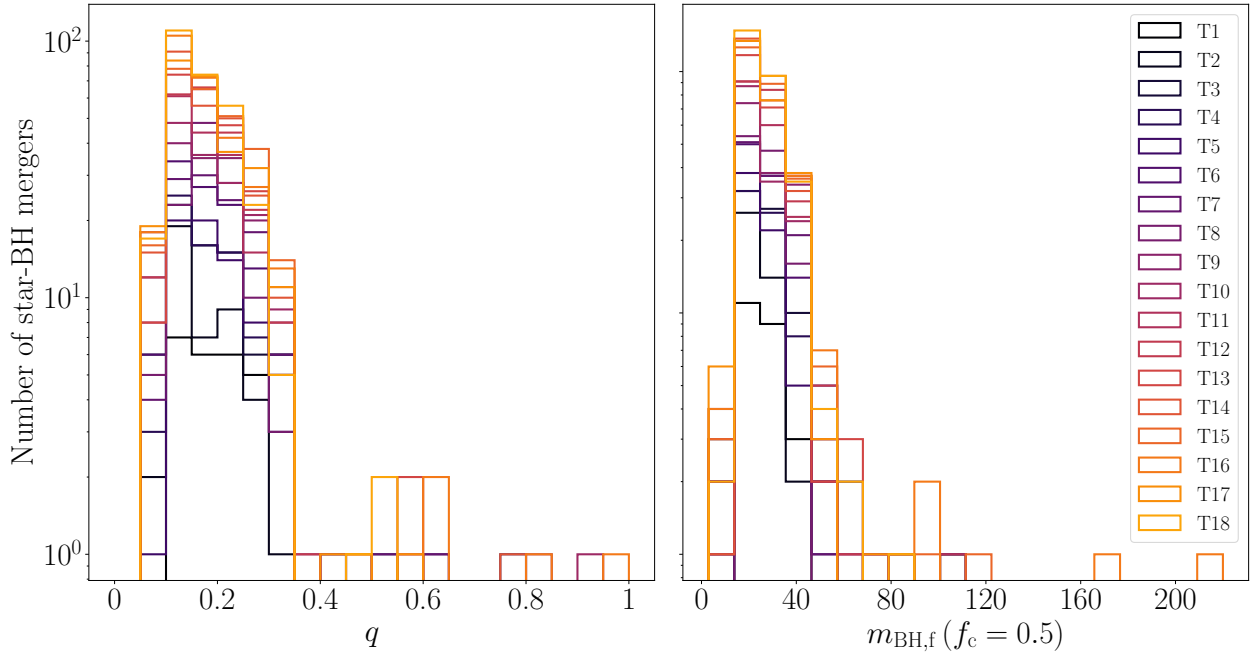


Fig. A.2: Mass-ratio q distribution of merging systems with a stellar primary and a BH secondary (left) and final BH mass assuming $f_c = 0.5$ (right), for all the simulated models.